Journal of Power Sources 239 (2013) 538–545

Contents lists available at SciVerse ScienceDirect

Journal of Power Sources

journal homepage: www.elsevier.com/locate/jpowsour

Surface structure and high-rate performance of spinel $Li_4Ti_5O_{12}$ coated with N-doped carbon as anode material for lithium-ion batteries

Haiquan Zhang, Qijiu Deng, Chengxu Mou, Zongling Huang, Ying Wang, Aijun Zhou, Jingze Li*

State Key Laboratory of Electronic Thin Films and Integrated Devices, School of Microelectronics and Solid-state Electronics, University of Electronic Science and Technology of China, Chengdu 610054, China

HIGHLIGHTS

- Individual N and C sources are applied to coat N-doped carbon layer on $Li_4Ti_5O_{12}$.
- This straightforward methodology is easy to optimize N/C ratio and carbon layer thickness.
- The N-doped C-coated $Li_4Ti_5O_{12}$ presents uniform or serrated surface structure.
- Surface modified samples display outstand electrochemical properties at high current rate.

ARTICLE INFO

Article history:
Received 25 February 2013
Accepted 4 March 2013
Available online 19 April 2013

Keywords:
Nitrogen-doped
Carbon-coating
Surface modification
Lithium titanate

ABSTRACT

We have reported a straightforward strategy to fabricate $Li_4Ti_5O_{12}$ composites coated with N-doped carbon layer by using NH_3 as N source and sugar as C source, which is a benefit for optimizing carbon layer thickness and tuning atomic ratio of N/C. The composite was synthesized by a conventional solid state reaction with ball milled mixture of TiO_2, Li_2CO_3, and sugar as the precursor, then followed by a high temperature annealing in the atmosphere of Ar and NH_3. The choice of titanium source has an impact on the $Li_4Ti_5O_{12}$ surface morphology as well as electrochemical properties. N-doped TiO_2 can lead to the generation of uniform N-doped C-coating layer, resulting in improved electrochemical performances at high current rate. The N-doped C-coating $Li_4Ti_5O_{12}$ obtained by using Anatase TiO_2 produces a serrated thin carbon layer, showing the best electrochemical behaviors with the discharge capacity of 100 mAh g^{-1} at high rate of 24 C and 92.2% of initial capacity after 800 cycles at 12 C, which should be one of the promising anode materials for hybrid electric vehicles.

1. Introduction

Three traditional energies including coal, oil and natural gas, soon are running out, which have brought about global warming and ecological environmental degradation [1,2]. Exploring renewable energy materials has become one of the most important trends all over the world. In recent years, rechargeable lithium ion batteries (LIBs) have attracted worldwide attention for the outstanding advantages such as high safety, high power density, long cycle life, fast charge/discharge properties and friendliness to the environment [3]. As a result, it is gradually becoming one of the most popular electrochemical energy storage devices to save those petrified energy sources and decrease the environmental burden. However, graphite used as a conventional anode in commercial LIBs displays quite slow Li^+ diffusion at low temperature, which results in serious kinetic problem under the condition of high rate charge/discharge [4]. In addition, Li^+ insertion/deinsertion potential of the graphite anode is below 0.2 V vs. Li/Li^+, which is near metallic lithium deposition potential, rendering the great possibility of internal electrical short for the batteries.

As an alternative to graphite, $Li_4Ti_5O_{12}$ (LTO) anode material has many promising characteristics, such as a relatively high potential plateau at about 1.55 V vs. Li/Li^+ for avoiding the formation of solid sate interphase (SEI) layer, a zero-strain insertion material for providing excellent long cycle life [3,5], the unique thermodynamic stability for promoting the safety [6]. All of these merits make LTO particularly attractive as the advanced anode material of high power LIBs for large-scale application. Nevertheless, the pretty low electronic conductivity (merely 10^{-13} S cm^{-1}) leads to serious electrochemical polarization at high current densities [7,8]. So far, various strategies have been proposed to resolve the issue of poor electronic conductivity and lessen the polarization, which

* Corresponding author. Tel.: +86 28 8320 7620; fax: +86 28 8320 2569.
E-mail addresses: lijingze@uestc.edu.cn, microenergy@uestc.edu.cn (J. Li).

0378-7753/$ – see front matter © 2013 Elsevier B.V. All rights reserved.
http://dx.doi.org/10.1016/j.jpowsour.2013.03.013

include reducing the particle size down to deca-nanometer scale by soft chemical methods (sol–gel, solvothermal synthesis, spray-drying, etc.) [9–12], doping with foreign metal or non-metal ions (Zn^{2+}, La^{3+}, Nb^{5+}, Mo^{6+}, Mg^{2+}, Ni^{3+}, Al^{3+}, Cr^{3+}, C_O^{3+}, Mn^{3+}, V^{5+}, F^-, Cl^- and Br^-) [7,13–18] and coating excellent electronic conductive matters (Ag, amorphous carbon, graphite and graphene) [19–21] on the surface. Among various methods, the well-known surface carbon-coating technique is one of the most effective ways to improve the rate performance of the electrode material. For instance, G. N. Zhu prepared carbon-coated (C-coated) LTO nano-porous microspheres by a spray drying method combined with high temperature annealing, and the corresponding discharge capacity is up to 126 mAh g^{-1} at a high current rate of 20C [20]. However, the simple C-coated LTO cannot satisfy the requirements of the practical application considering either high rate electrochemical performance or volume energy density because of the difficultly in enhancing electrical conductivity of the coated carbon film itself, forming a defect-free coating layer, etc. To overcome these crucial issues, some researchers have reported a new surface coating technique using the precursor containing carbon and nitrogen elements to deposit a very thin film on the LTO surface. The nitrogen-doped (N-doped) carbon forms a perfect consecutive electronic conductive layer, and effectively improves the rate performance. Recently, Y.S. Hu has proposed several organic species where one material contains at least carbon and nitrogen elements, namely pyridine [22], ionic liquids [23] and urea [24], as N-doped carbon precursor, which greatly enhanced the surface electrical conductivity and optimized the electrical contact within the electrode.

In the work reported here, we developed a simple method to coat N-doped carbon layer on LTO particles, where C and N elements were independently from different precursors. Sugar was applied as C source [25], which is mixed with TiO_2 and Li_2CO_3 for a solid-state reaction. Different from conventional carbon coating process, the high temperature annealing was done in the atmosphere of NH_3 [26], resulting in the formation of N-doped carbon layer. This straightforward methodology had the advantage to easily optimize the ratio of N/C and the carbon layer thickness. Furthermore, we found the surface state of TiO_2 precursor played an important role in the quality of the coated carbon layer.

2. Experimental

2.1. Material preparation

All the chemicals were of analytical grade. The spinel LTO was synthesized via a simple solid state reaction, which is easy to be scale-up for industrial production. In terms of the type of titanium source, the synthesis methodologies were classified as solid-state processes I and II, as shown in Scheme 1. As for solid-state process I, anatase TiO_2 as titanium source and Li_2CO_3 as lithium source

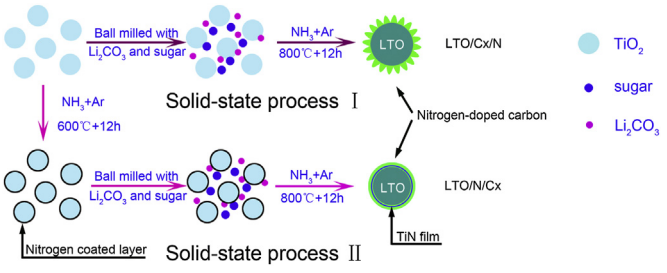

Scheme 1. Schematic illustration for the synthesis of the LTO/C20/N and LTO/N/C20 compounds.

were firstly weighted with Li:Ti molar ratio of 4:5. Secondly, the mixture was ball milled with sugar as carbon source while sugar:TiO_2 weight ratio was varied from 10:100, 20:100 to 30:100. Finally, the well-milled precursor was annealed at 800 °C for 12 h in the mixed atmosphere of Ar and HN_3, in which $NH_3 \cdot H_2O$ was applied as nitrogen source. The obtained samples were labeled as LTO/Cx/N (x = 10, 20, and 30), respectively. The solid-state process II was same as solid-state process I, except that TiO_2 raw material was pre-treated under 600 °C for 3 h in a mixed atmosphere of Ar and HN_3 so as to form N-doped TiO_2. Correspondingly, the synthesized final products were labeled as LTO/N/Cx (x = 10, 20, and 30).

2.2. Material characterization

The crystalline phases of LTO composites were identified by X-ray diffraction using Co Kα radiation (XRD, λ = 1.7890 Å, X'Pert Pro MPD) with a step size of 0.03° (2θ) in the range of 18–85°. The morphologies of the samples were observed using a field-emission scanning electron microscope (FE-SEM, Hitachi, S3400N) and transmission electron microscope (TEM, JEOL, JEM-100CX). The lattice images were collected with a high-resolution transmission electron microscope (HR-TEM, FEI, Tecnai F20). The components of the coated layers were analyzed with a Fourier Transform Infrared Spectrometer system (IR, IRrestige-21).

2.3. Cell assembling and electrochemical test

The electrochemical properties of the active materials were measured by assembling half cells. The LTO working electrode was prepared by casting N-methyl-2-pyrrolidine (NMP) slurry onto a Cu foil with the active material, carbon black as conducting additive and polyvinylidene fluoride (PVDF) as the binder at a weight ratio of 8:1:1. Subsequently, the electrode was dried under vacuum at 110 °C for 24 h. The test cell was assembled in an Ar filled glove-box using lithium metal foil and polypropylene (PP) membrane (Celgard 2400) as the counter electrode and the separator, respectively. And the electrolyte was 1 mol L^{-1} $LiPF_6$ dissolved in a mixture of ethylene carbonate (EC), diethyl carbonate (DEC) and dimethyl carbonate (DMC) (1:1:1 by volume). The charge/discharge measurements were carried out under desired current densities with the voltage between 1.0 and 3.0 V by using a CT2001A cell test instrument (LAND Electronic Co.) at room temperature. Cyclic voltammograms (CV) were performed from 1.0 to 3.0 V at different scanning rates using Solartron SI1287.

3. Results and discussion

Fig. 1 shows XRD curves of all of LTO based products. As the references, pristine LTO and N-doped LTO and C-coated LTO were synthesized, and the corresponding XRD patterns were shown in Fig. 1a and Fig. 1b. It is apparent that the most intense diffraction peaks appear at 21.5, 41.7, 50.7 and 74.5°, which are indexed to (111), (311), (400) and (440) planes of a face-centered cubic spinel LTO (JCPDS card no. 49-0207), respectively. This result indicates that the main phase of all the products is spinel LTO with Fd3m space group. In order to see the trivial effect of the coated material on the LTO crystalline structure, silica fume (JCPDS card no. 27-1402) was used as internal standard to calibrate the systematical error of the XRD analytical equipment. As a consequence, each of XRD profiles demonstrates a set of strong peaks ascribed to Si crystal. All of the XRD curves were then shifted in light of the peak position of Si (111) plane. Correspondingly, the detail of the strongest peak representing LTO (111) plane was exhibited in Fig. 1c and d. It is obvious that the central position of this peak

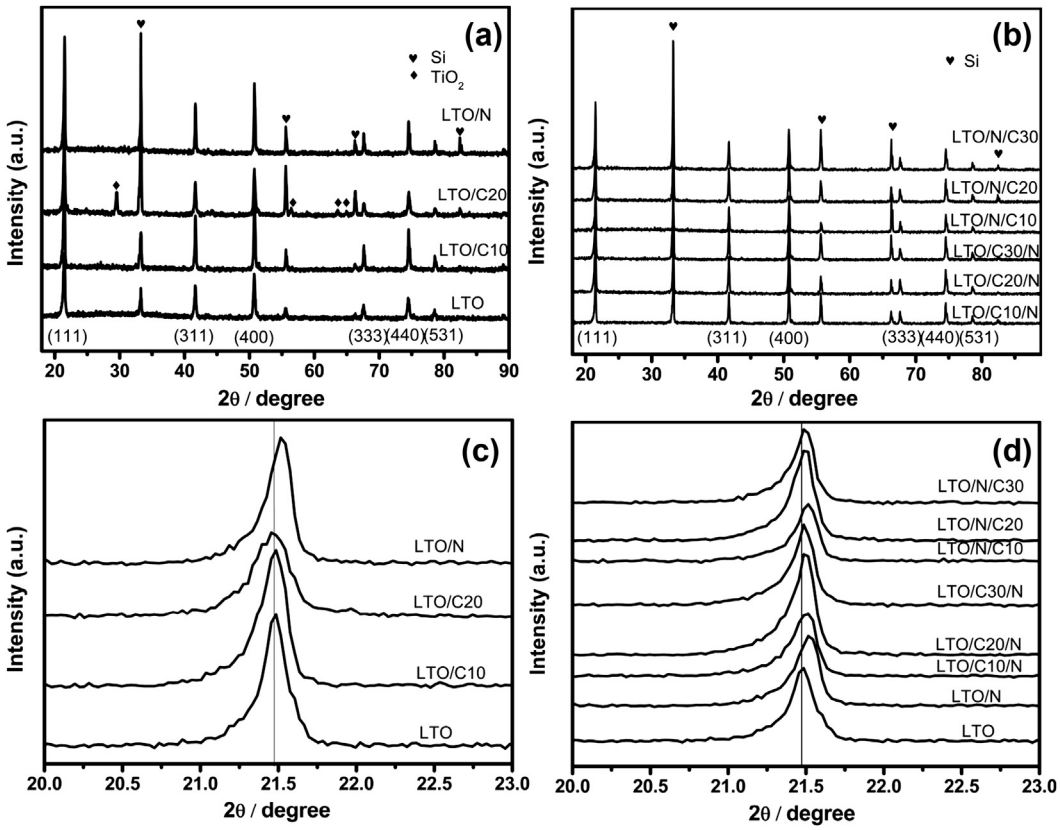

Fig. 1. (a) and (b) XRD patterns of the pristine $Li_4Ti_5O_{12}$, the N-doped and C-coated LTO. (c) and (d) The enlarged (1 1 1) peaks of the pristine $Li_4Ti_5O_{12}$ and coated LTO powders.

moves toward the direction of high angle after solely doping of N atom (N-doped LTO), indicating the N atoms might be doped in the LTO lattice and lead to the formation of a thin layer of new material such as TiNx [26]. On the contrary, the C-coated LTO does not change the peak position despite that the carbon content in the precursors was varied. This result implies that the carbon atoms are not diffused into the bulk phase of LTO particles. However, the N-doped C-coated LTO shows different tendencies, where the peak position is sensitive to the carbon content. That is to say, the higher carbon content can decrease the peak shift distance. It can be easily deduced that the doped N atoms and the coated C atoms should take a chemical reaction leading to the N bonded C atoms through sp^3 and sp^2 hybridization in the carbon film, which is similar to the previously reported N-doped carbon film [27]. As for LTO/N/Cx, N atoms which stay in the lattice of spinel LTO might slowly diffuse toward the surface during the thermal treating process, then react with the contacted carbon film on the LTO surface, resulting in the formation of N doped carbon layer in the vicinity of LTO surface as well as the reduced concentration of N atoms in LTO. Since the total number of the doped N atoms is quite limited, it is very possible that the thicker C-coating film can consume up all of the doped N atoms. This is the reason why the peak position of LTO/N/C20 and LTO/N/C30 does not move with respect to the pristine LTO. Alternatively, the carbon film might hinder N atoms access native LTO surface in the case of LTO/Cx/N since a favorable chemical reaction occurs between the N element and C element in the bulk phase of the coated carbon layer. Hence, N atoms might be difficult to penetrate the thicker carbon film for approaching LTO, leading to the LTO surface is not effectively doped by N atoms. The above results give a hint that the N doped carbon layer is apt to form a perfect coating layer surrounding the LTO particles.

IR spectra of the pristine and surface-modified LTO materials are shown in Fig. 2. The IR profile of LTO/N is very similar to that of pristine LTO, where all of the peaks can be assigned to vibration mode of pristine LTO. After the LTO surface was modified with the N-doped carbon layer, additional peaks were observed. A sharp peak appears at 1650 cm^{-1} for both LTO/N/C20 and LTO/C20/N, which can be attributed to C═N bond [28–30]. Furthermore, the LTO/N/C20 sample presents an IR absorption peak at 2360 cm^{-1}, which is corresponding to C≡N bond [28]. These evidences clarify that the coating layer consists of N-doped carbon with at least two bonding ways between C and N atoms.

Fig. 3 exhibits SEM images of the pristine LTO, N-doped LTO/N, C-coated LTO/C10, LTO/N/C20 and LTO/C20/N samples. All the LTO particles prepared at 800 °C are uniform, and their size is around 200–600 nm. It is clear that the size distribution of the modified LTO particles is not greatly influenced by N-doping, C-coating, and N/C treating processes.

The coating structure on the surface of LTO materials was clearly clarified by TEM and HR-TEM. Fig. 4 reveals TEM images of LTO/N, LTO/N/C20 and LTO/C20/N samples. LTO/N shows a very smooth surface, indicating there does not exist external coating layer. Compared to the N-doped LTO, both of the LTO/N/C20 and LTO/C20/N materials are covered by a very thin carbon film on the LTO surface.

To further examine the architecture of the N-doped and C-coated $Li_4Ti_5O_{12}$ samples, HR-TEM measurements were carried out. HR-TEM images of the LTO/N, LTO/N/C20 and LTO/C20/N samples are shown in Fig. 5. Both of the LTO/N/C20 and LTO/C20/N species are surrounded by a thin layer of amorphous carbon with the thickness of about 1–5 nm. In the case of the LTO/C20/N product, the N-doped carbon layer with excellent electronic conductive capability presents serration-like morphology whose height and

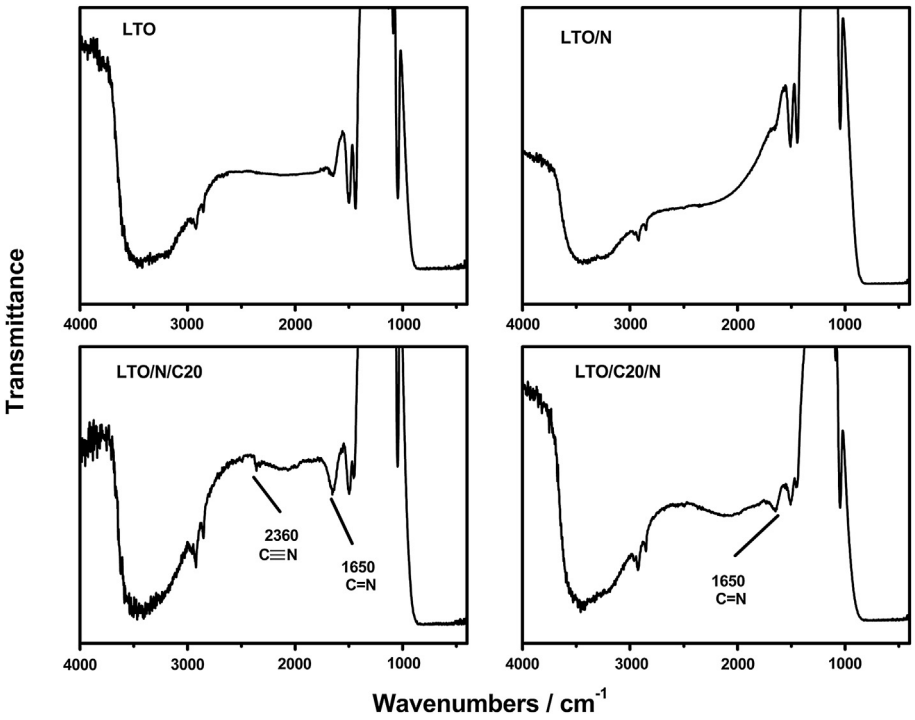

Fig. 2. FI–IR spectra of pure LTO, LTO/N, LTO/N/C20 and LTO/C20/N samples.

breadth are ca. 1–5 nm and 1–5 nm, as shown in Fig. 5b. However, a very uniform N-doped carbon layer with the thickness of ca. 4 nm is formed on the surface of the LTO/N/C20 sample as displayed in Fig. 5c, which has a compact structure typical of graphitized carbon.

To understand the effect of N-doping treatment on the morphology of the coated carbon layer, selected area electron diffraction (SAED) patterns of the N-doped and/or C-coated LTO samples were recorded, as explicated in Fig. 6. The TiNx species is discovered in the LTO/N and LTO/N/C20 samples, whereas it does not appear in the LTO/C20/N sample. According to the HR-TEM and SAED results of the LTO/N/C20 sample, it can be concluded that the melted sugar solvent might spread over the whole surface of the $TiNx/TiO_2$ particles on the initial stage of the carbon coating process, then the released N atoms from TiNx transition layer will react with the surrounding carbon atoms, resulting in the formation of a uniform compact coating layer under the mixed atmosphere of Ar and NH_3. On the other side, the LTO/C20/N material reveals a serrated surface because of the absence of TiNx transition layer.

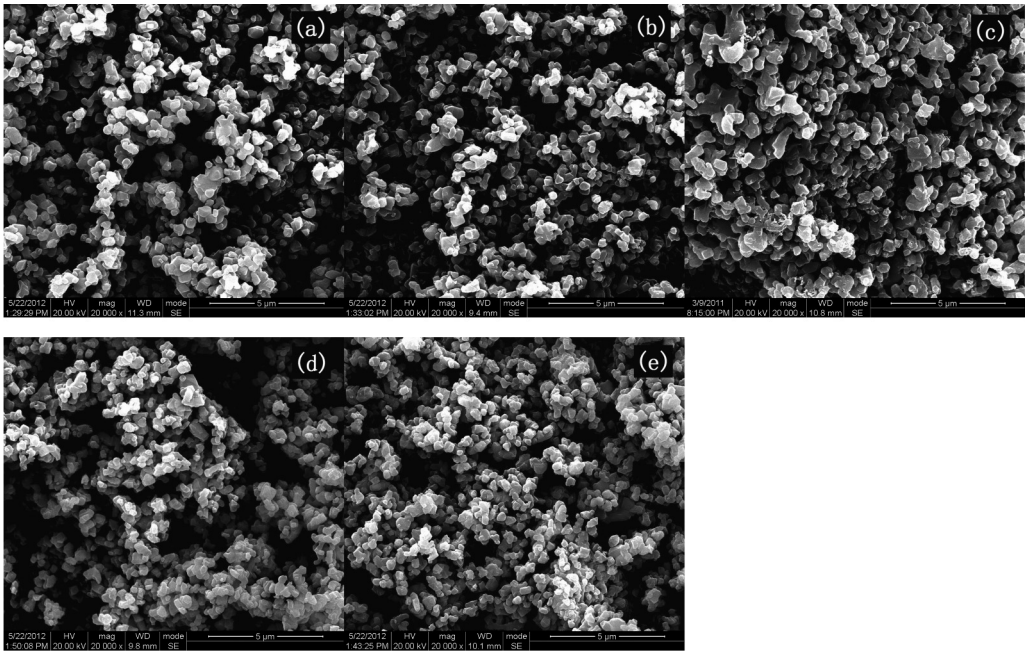

Fig. 3. SEM images of the pristine LTO sample (a), the N-doped LTO/N sample (b), the C-coated LTO/C10 (c), the N-doped and C-coated LTO/C20/N (d) and LTO/N/C20 (e) electrodes.

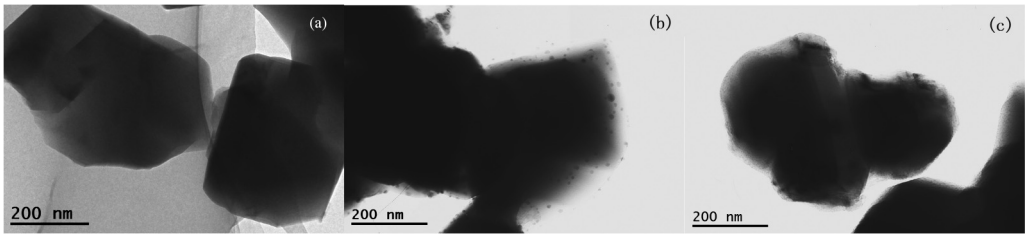

Fig. 4. TEM images of the N-doped LTO/N sample (a), the coated LTO/C20/N (b) and LTO/N/C20 (c) samples.

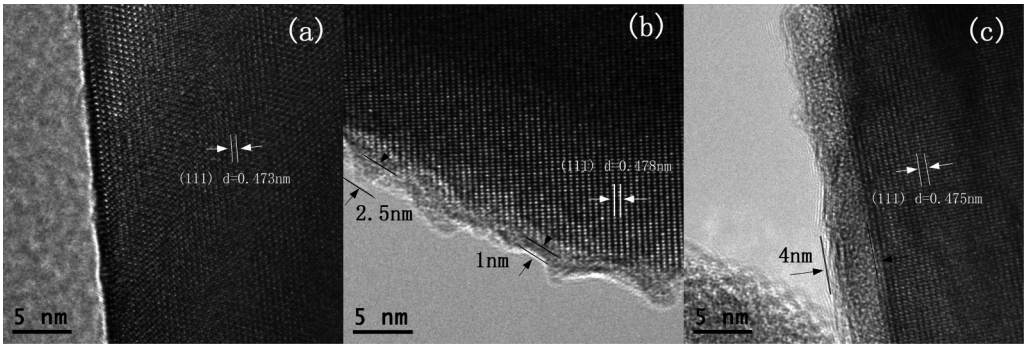

Fig. 5. HRTEM images of the LTO/N (a), the LTO/C20/N (b) and LTO/N/C20 (c) materials.

The charge/discharge curves of the coated LTO composites are shown in Fig. 7 at different current densities to evaluate the capacity–rate relationship. Fig. 7a and b displays the rate capability of the N-doped C-coated samples with the voltage limits of 1–3 V as a function of the nominated carbon content. At a low rate of 0.5 C, all of the N-doped C-coated samples reach nearly the same reversible capacity around 170 mAh g^{-1}. As for LTO/N/Cx series, LTO/N/C20 with approximately 4 wt% of the N-doped carbon compound, which was calculated according to the weight loss at 600 °C, shows the best electrochemical performance at the elevated current rate. With the current rate increasing from 1C, 3C, 6C, 12C, to 24C, the specific capacity slowly decreases to 158, 145, 132, 118 and 100 mAh g^{-1}, respectively. On the other hand, the discharge capacity of the LTO/C20/N product with about 3.5 wt% of the N-doped carbon layer is 158, 148, 138, 125 and 110 mAh g^{-1} at 1 C, 3 C, 6 C, 12 C and 24 C, respectively. It is obvious that the electrochemical performance of LTO/C20/N is better than those of LTO/C10/N and LTO/C30/N. In a sentence, the rate capability of the N-doped C-coated LTO is not proportional to the carbon content, which determines the thickness and the conductivity of the N-doped carbon layer. The thicker film provides higher conductivity, whereas hinders Li^+ ion transfer during the charge/discharge process. Therefore, an optimized film with very thin thickness might be approached while the quality of the coating film is improved by doping of N elements, which is a benefit for the enhanced weight and energy densities of the batteries.

The rate performances of the pristine LTO, LTO/N, LTO/C10, LTO/N/C20 and LTO/C20/N active electrodes are summarized in Fig. 7c. Compared to the pristine LTO, LTO/N and LTO/C electrodes, the rate performance of the N-doped C-coated samples is much better. It is noteworthy that the capacity (110 mAh g^{-1}) of LTO/C20/N at the 24C high rate is even larger than the capacity (105 mAh g^{-1}) of the pristine LTO sample at the 3C rate. It might be due to the high intrinsic conductivity of N-doped carbon film [22–24,31]. Moreover, the reversible capacities of LTO/C20/N are appreciably higher than LTO/N/C20 while the current rate is over 6C. This result points out that the exceptional serrate structure of LTO/C20/N has the advantage on the promotion of electrochemical kinetics behavior over the uniform carbon layer of LTO/N/C20. Interestingly, LTO/C20/N with optimized N/C ratio shows better rate performances than conventional N-doped C-coated LTO using only one specie as the N and C precursor such as urea [24,31], ionic liquid (1-ethyl-3-methylimidazolium dicyanamide) [23].

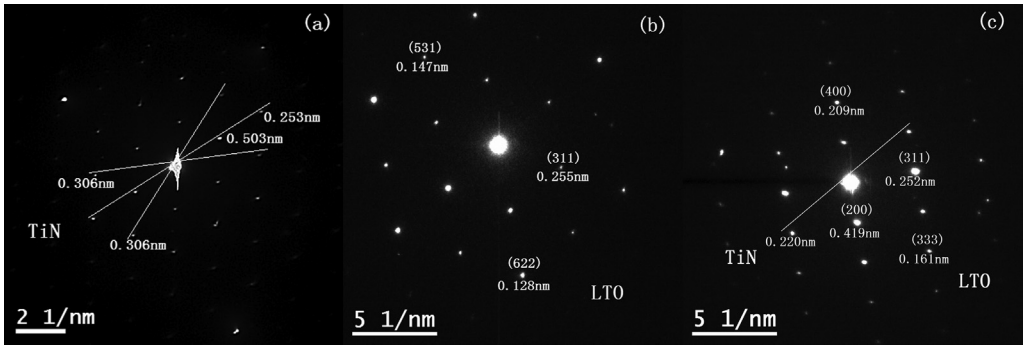

Fig. 6. SAED images of the N-doped LTO/N sample (a), the coated LTO/C20/N (b) and LTO/N/C20 (c) samples.

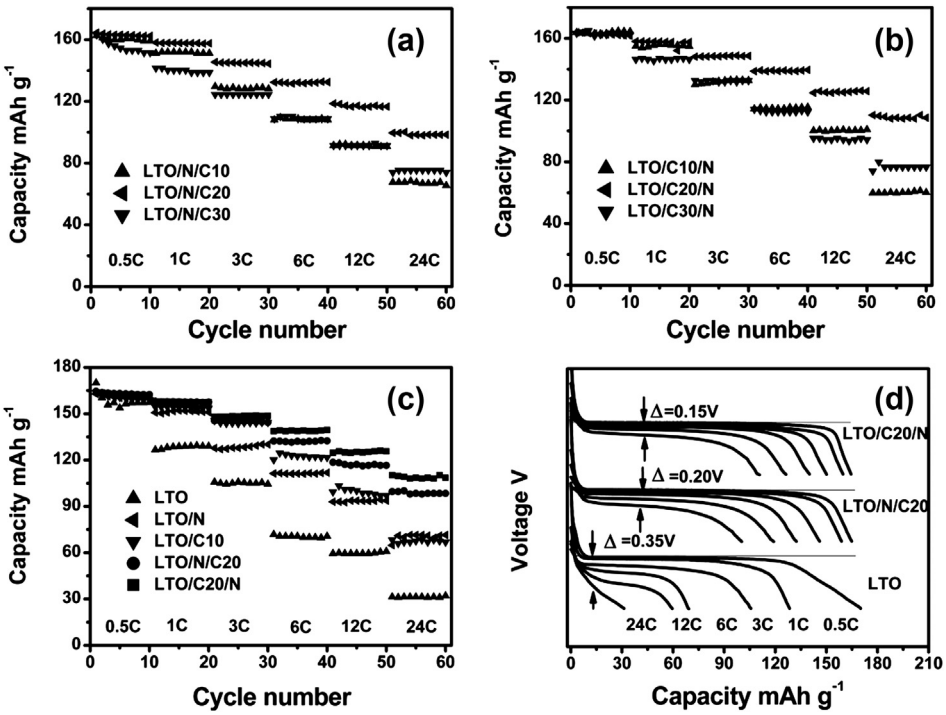

Fig. 7. (a), (b) and (c) Specific capacity of the N-doped and C-coated LTO compounds at different rates. (d) Discharge curves of the pristine LTO, the coated LTO/C20/N and LTO/N/C20 samples.

Fig. 7d displays the typical discharge curves of LTO, LTO/N/C20, and LTO/C20/N at different current rate. It is apparent that all electrodes at low current rate of 0.5C and 1C reveal flat operation potential plateaus about 1.5 V vs. Li/Li$^+$. However, the potential plateau of the pristine LTO becomes shorter and slightly bends down at the elevated current rates while that of N-doped C-coated electrodes still remains flat. Especially, the polarizing voltages between the practical and theoretical discharge plateau (1.55 V) are only 0.2 V and 0.15 V for LTO/N/C20 and LTO/C20/N, respectively, which are significantly lower than that of the pristine LTO electrode (0.37 V). The principal result further indicates that the kinetic performance at high current rate is definitely improved by N-doped carbon coating of LTO.

Fig. 8 displays cyclic performance of the pristine LTO, LTO/C20/N and LTO/N/C20 at 12C. As shown in Fig. 8a, stable cycling plots are observed for the LTO/N/C20 and LTO/C20/N samples. The corresponding specific discharge capacities are 126 and 116 mAh g^{-1} in the initial cycle, and remain at 111 and 107 mAh g^{-1} after 800 charge/discharge cycles, keeping 88.1% and 92.2% retention of the initial capacities. However, as exhibited in Fig. 8a, the first discharge capacity of the pristine spinel LTO electrode is 60 mAh g^{-1}. The capacity after 800 cycles is quickly down to 25 mAh g^{-1} with 42% maintenance of the initial discharge capacity. Furthermore, Fig. 8b illustrates the relationship between cycle number and columbic efficiencies of the pristine and N-doped C-coated LTO materials. The columbic efficiency is very close to 100% although the cycle number is up to 800. While reconsidering the cycling performance of pristine LTO, it can be concluded that the capacity decline occurs during the charge process, i.e., Li$^+$ insertion process. The poor electronic conductivity of pristine LTO might be the key factor to hinder the charge transfer, resulting in the increased polarization cycle by cycle. The extraordinary cycling performance of the N-doped C-coated LTO proves that the N-doped carbon layer can construct the pathways for effectively transferring the electrons even under the high charge/discharge rate, which can do a favor for quick migration of the inserted Li$^+$ ion and reducing the polarization.

To precisely figure out the influence of N-doped carbon layer on the kinetic performance, cyclic voltammograms (CV) of the pristine LTO, LTO/N/C20 and LTO/C20/N were shown in Fig. 9a–c. The redox peaks of the LTO/N/C20 sample are the broadest at the same scan rate. As a contrast, the peak current of the pristine LTO is the highest at the same scan rate. These results demonstrate that the uniform compacted carbon layer of LTO/N/C20 impedes Li$^+$ diffusion, and the dentate surface structure of LTO/C20/N has a very slight effect on the ion transferring between the electrolyte and the bulk LTO phase. Fig. 9d displays the correlation between the anodic peak currents and the square roots of the scan rate for these LTO based electrodes, which matches the linear relationship very well.

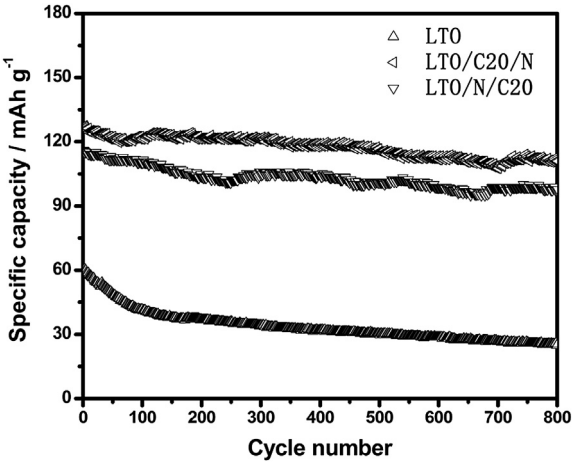

Fig. 8. Cycling performances of the pristine LTO sample, the coated LTO/C20/N and LTO/N/C20 samples at 12C.

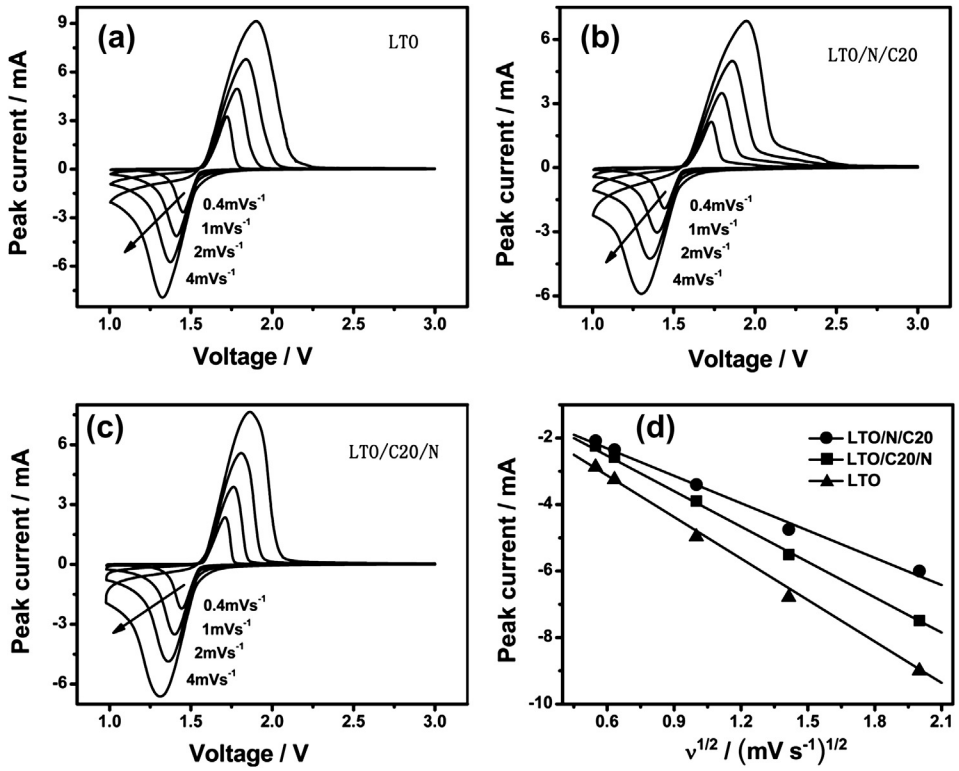

Fig. 9. Cyclic voltammograms of pure LTO (a), LTO/N/C20 (b) and LTO/C20/N (c), (d) peak current against square root of scan rate for these three samples.

It is the typical behavior of diffusion-controlled electrode reaction process. The diffusion coefficient can be estimated based on the slope of the oblique line. Hence it can be easily deduced that the pristine LTO has the largest diffusion coefficient, and LTO/N/C20 has the smallest. Since these three materials have almost the same particle size distribution, the reduced diffusion coefficients of LTO/N/C20 and LTO/C20/N should be attributed to the coated layer. As a consequence, the compact uniform N-doped carbon layer of LTO/N/C20 can seriously reduce Li^+ insertion/deinsertion rate. As for LTO/C20/N, the unique dentate structure with a relatively thin carbon layer might reduce the barrier for Li^+ transportation, rendering relatively high Li^+ mobility.

To understand the improved high-rate performance for N-doped C-coated LTO hybrid materials, we also measured electrochemical impedance spectroscopy (EIS) of the pure $Li_4Ti_5O_{12}$, LTO/N/C20 and LTO/C20/N, as shown Fig. 10. The spectra of the pure LTO electrode consists of a semicircle at high-middle frequencies attributed to the charge-transfer reaction and an oblique linear Warburg part at low frequencies attributed to the Li^+ diffusion. These impedance spectra were fitted by ZView software using an equivalent circuit mode, shown in the inset of the figure. Here R_s and R_{ct} represent the solution resistance and charge transfer resistance at the particle/electrolyte interface, respectively. CPE represents a constant phase element and C_L is placed to represent the double-layer capacitance. Table 1 displays some of the parameters obtained by fitting. It can be observed that R_s of the coated LTO/N/C20 and LTO/C20/N samples are similar to the pure LTO, whereas the surface modified LTO materials exhibit much lower charge transfer resistance R_{ct} than that of the pristine LTO electrode. Furthermore, the exchange current density ($i_0 = RT/nFR_{ct}$) of the coated LTO/N/C20 and LTO/C20/N hybrid materials is higher than pure LTO product. Therefore, the lowered charge transfer resistance of the modified electrodes further proves that N-doped carbon surface layer can improve electrical conductivity of the insulating LTO particles.

Based on the above discussion, it is possible to figure out why LTO/C20/N shows the best rate performance with respect to pure phase LTO, LTO/N, LTO/C, LTO/N/C20. Firstly, N-doped carbon film has higher conductivity than pure carbon film, leading to higher exchange current density. Secondly, LTO/C20/N has the thinnest coating layer, offering a reasonable Li^+ diffusion coefficient. Thirdly, LTO/C20/N might have the lowest concentration of the doped N atoms, offering the largest amount of the electrochemical active material. Shortly speaking, the N-doped C-coated LTO/C20/N might

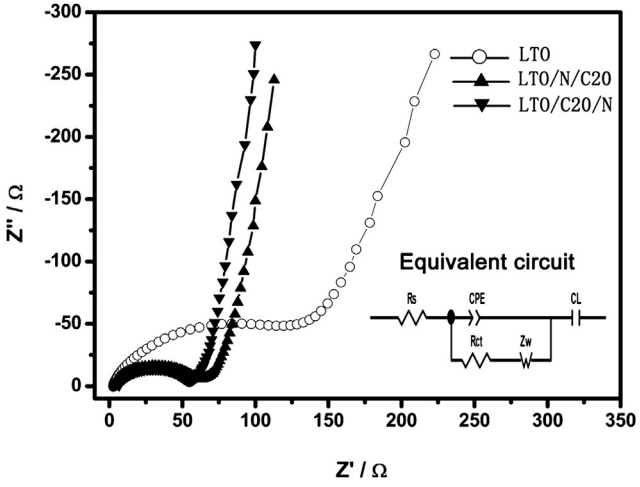

Fig. 10. EIS spectra and equivalent circuit model for the pure LTO, LTO/N/C20 and LTO/C20/N samples.

Table 1
Impedance parameters of the pure LTO, surface modified LTO/N/C20 and LTO/C20/N electrodes calculated by equivalent circuit modeling.

Materials	R_s (Ω)	R_{ct} (Ω)	i_0 (mA cm^{-2})
$Li_4Ti_5O_{12}$	2.775	119.3	0.21
LTO/N/C20	3.571	62.08	0.41
LTO/C20/N	6.637	54.72	0.46

keep the balance between electrical conductivity and ionic conductivity, yielding superior comprehensive electrochemical properties at high current rate.

4. Conclusions

The general principle to design the qualified coating layer has herein been discussed. The key point is to set a suitable balance point between the electrical conductivity and the ionic conductivity of the coated layer. N-doped carbon film was synthesized due to its relatively high electrical conductivity, where NH_3 and sugar were adopted as nitrogen and carbon sources, respectively. The electrical conductivity was adjusted by changing the weight ratio of C/TiO_2 from 10/100, 20/100, to 30/100. On the other hand, Li^+ mobility was modulated by the type of titanium source such as TiO_2, N-doped TiO_2. N-doped TiO_2 as titanium source could produce a uniform thin N-doped carbon layer, and anatase TiO_2 as titanium source could generate a serrated carbon thin layer. At a high discharge current rate of 24C, the specific capacities of the coated LTO/N/C20 and LTO/C20/N samples reach nearly 100 and 110 mAh g^{-1}, and their polarizing voltages are only 0.2 V and 0.15 V, respectively. The excellent electrochemical performances make the LTO/C20/N sample become a promising anode material for high-rate LIBs and the straightforward solid-state synthesizing routine enables the mass production of large quantities.

Acknowledgments

This work was supported by funding from NSFC (nos. 21073029, 11234013, 51211140045), RFDP (no. 20100185110019), Program for New Century Excellent Talents in University (no. NCET-10-0296), Fundamental Research Funds for the Central Universities (no. ZYGX2012Z003). The authors thank Miss Ming Liu, working at Analytical and Testing Center of Sichuan University, China, for her help in TEM characterization.

References

[1] A.J. Davis, L.S. Jenkinson, J.H. Lawton, B. Shorrocks, S. Wood, Nature 391 (1998) 783–786.
[2] C. Packer, R. Hilborn, A. Mosser, B. Kissui, M. Borner, G. Hopcraft, J. Wilmshurst, S. Mduma, A.R.E. Sinclair, Science 307 (2005) 390–393.
[3] M.S. Whittingham, Chem. Rev. 104 (2004) 4271–4301.
[4] J. Chen, L. Yang, S. Fang, S.-i. Hirano, K. Tachibana, J. Power Sources 200 (2012) 59–66.
[5] L. Aldon, P. Kubiak, M. Womes, J.C. Jumas, J. Olivier-Fourcade, J.L. Tirado, J.I. Corredor, C.P. Vicente, Chem. Mater. 16 (2004) 5721–5725.
[6] T.-F. Yi, Y. Xie, Y.-R. Zhu, R.-S. Zhu, H. Shen, J. Power Sources 222 (2013) 448–454.
[7] C.H. Chen, J.T. Vaughey, A.N. Jansen, D.W. Dees, A.J. Kahaian, T. Goacher, M.M. Thackeray, J. Electrochem. Soc. 148 (2001) A102–A104.
[8] A. Guerfi, P. Charest, K. Kinoshita, M. Perrier, K. Zaghib, J. Power Sources 126 (2004) 163–168.
[9] J. Gao, C.Y. Jiang, J.R. Ying, C.R. Wan, J. Power Sources 155 (2006) 364–367.
[10] Z.Y. Wen, Z.H. Gu, S.H. Huang, J.H. Yang, Z.X. Lin, O. Yamamoto, J. Power Sources 146 (2005) 670–673.
[11] J. Huang, Z. Jiang, Electrochem. Solid-State Lett. 11 (2008) A16–A18.
[12] S.-H. Yu, A. Pucci, T. Herntrich, M.-G. Willinger, S.-H. Baek, Y.-E. Sung, N. Pinna, J. Mater. Chem. 21 (2011) 806–810.
[13] T.-F. Yi, H. Liu, Y.-R. Zhu, L.-J. Jiang, Y. Xie, R.-S. Zhu, J. Power Sources 215 (2012) 258–265.
[14] J. Gao, C. Jiang, C. Wan, J. Electrochem. Soc. 157 (2010) K39–K42.
[15] T.-F. Yi, Y. Xie, Q. Wu, H. Liu, L. Jiang, M. Ye, R. Zhu, J. Power Sources 214 (2012) 220–226.
[16] T.-F. Yi, Y. Xie, J. Shu, Z. Wang, C.-B. Yue, R.-S. Zhu, H.-B. Qiao, J. Electrochem. Soc. 158 (2011) A266–A274.
[17] Z. Yu, X. Zhang, G. Yang, J. Liu, J. Wang, R. Wang, J. Zhang, Electrochim. Acta 56 (2011) 8611–8617.
[18] T.-F. Yi, J. Shu, Y.-R. Zhu, X.-D. Zhu, R.-S. Zhu, A.-N. Zhou, J. Power Sources 195 (2010) 285–288.
[19] N. Zhu, W. Liu, M. Xue, Z. Xie, D. Zhao, M. Zhang, J. Chen, T. Cao, Electrochim. Acta 55 (2010) 5813–5818.
[20] G.-N. Zhu, H.-J. Liu, J.-H. Zhuang, C.-X. Wang, Y.-G. Wang, Y.-Y. Xia, Energy Environ. Sci. 4 (2011) 4016–4022.
[21] Y. Shi, L. Wen, F. Li, H.-M. Cheng, J. Power Sources 196 (2011) 8610–8617.
[22] Z. Ding, L. Zhao, L. Suo, Y. Jiao, S. Meng, Y.-S. Hu, Z. Wang, L. Chen, Phys. Chem. Chem. Phys. 13 (2011) 15127–15133.
[23] L. Zhao, Y.-S. Hu, H. Li, Z. Wang, L. Chen, Adv. Mater. 23 (2011) 1385–1388.
[24] H. Pan, L. Zhao, Y.-S. Hu, H. Li, L. Chen, ChemSusChem 5 (2012) 526–529.
[25] G.J. Wang, J. Gao, L.J. Fu, N.H. Zhao, Y.P. Wu, T. Takamura, J. Power Sources 174 (2007) 1109–1112.
[26] K.-S. Park, A. Benayad, D.-J. Kang, S.-G. Doo, J. Am. Chem. Soc. 130 (2008) 14930–14931.
[27] H. Niwa, K. Horiba, Y. Harada, M. Oshima, T. Ikeda, K. Terakura, J.-i. Ozaki, S. Miyata, J. Power Sources 187 (2009) 93–97.
[28] H.Z. Zhao, X.L. Chen, C.C. Jia, T. Zhou, X.H. Qu, J.K. Jian, Y.P. Xu, Mater. Sci. Eng. B – Solids 122 (2005) 226–230.
[29] Q. Lv, C.B. Cao, C. Li, J.T. Zhang, H.X. Zhu, X. Kong, X.F. Duan, J. Mater. Chem. 13 (2003) 1241–1243.
[30] Q.X. Guo, Y. Xie, X.J. Wang, S.Y. Zhang, T. Hou, S.C. Lv, Chem. Commun. (2004) 26–27.
[31] H.-Q. Gao, X.-Y. Wang, Z.-A. Zhang, Y.-Q. Lai, J. Li, Y.-X. Liu, J. Inorg. Mater. 25 (2010) 983–988.